

Influence of Different Iodide Salts on the Performance of Dye-Sensitized Solar Cells Containing Phosphazene-Based Nonvolatile Electrolytes

Seung-Hyun Anna Lee,[†] Anne-Martine S. Jackson,[†] Andrew Hess,[†] Shih-To Fei,[†] Sean M. Pursel,[‡] James Basham,[§] Craig A. Grimes,[§] Mark W. Horn,[‡] Harry R. Allcock,[†] and Thomas E. Mallouk^{*,†}

Departments of Chemistry, Engineering Science and Mechanics, and Electrical Engineering, The Pennsylvania State University, University Park, Pennsylvania 16802

Received: June 30, 2010; Revised Manuscript Received: July 28, 2010

Polyphosphazene-based electrolytes containing different iodide salts were studied as components of dye-sensitized solar cells (DSSCs). Electrolytes based on hexa[methoxyethoxyethoxycyclophosphazene] (MEE trimer) with dissolved LiI, NaI, NH₄I, and 1-methyl-3-propylimidazolium (PMII) and I₂ were examined by ac conductivity and steady-state voltammetry. These measurements gave the individual conductivities of I⁻, I₃⁻, and cations in each electrolyte as a function of salt concentration. The anionic conductivities were highest in the PMII system and decreased in the order PMII > NH₄I > NaI > LiI. Photovoltaic measurements of DSSCs containing these electrolytes showed the same order of performance, and electrochemical impedance spectra (EIS) under open circuit and forward bias conditions were used to study the separate impedance components of the cells. High polymeric polyphosphazene–plasticizer blends with a dissolved PMII/I₂ electrolyte gave better performance in DSSCs than equivalent poly(ethylene oxide)–plasticizer electrolytes. Although the efficiencies of these DSSCs were low (1.9%), this study identified the primary loss mechanisms and suggested possible avenues for designing more efficient polyphosphazene-based cells.

Introduction

Dye-sensitized solar cells (DSSCs) are promising solar conversion devices that can achieve >10% solar conversion efficiency using inexpensive and abundant materials.¹ However, volatile liquid electrolytes, which give the highest efficiency DSSCs, present problems for manufacturing and long-term stability. For DSSCs to become competitive with solid state solar cells, critical issues such as the leakage and evaporation of the volatile electrolyte must be addressed and overcome. Several different strategies for replacing organic electrolytes with room temperature ionic liquids,² organic hole transport materials,³ inorganic hole conductors,⁴ and polymer/redox couple blends⁵ have been proposed. In general, the efficiencies of DSSCs with these alternative electrolytes or hole conductors are substantially lower than those that contain low-viscosity liquid electrolytes.

Polyphosphazenes are inorganic polymers in which the backbone contains phosphorus–nitrogen repeating units. They are thermally and oxidatively stable and can accommodate a wide variety of functional side groups that enable a broad range of applications.^{6,7} The P–N repeating unit in polyphosphazenes, which is isoelectronic with the Si–O unit in siloxane polymers, confers high chain flexibility, resulting in low crystallinity and in low *T_g* values.⁸ This property leads to high lithium ion mobility with dissolved Li⁺ salts, and in fact polyphosphazene derivatives with oligo(ethyleneoxy) side chains show higher Li⁺ mobility than poly(ethylene oxide) and are promising materials for lithium ion battery applications. Because lithium iodide/triiodide is the most commonly used electrolyte salt in DSSCs,

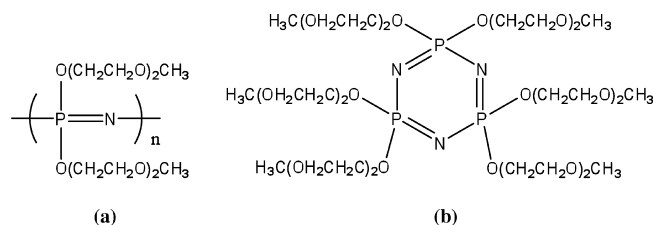


Figure 1. Structures of (a) methoxyethoxyethoxypolyphosphazene (MEEP) and (b) hexa[methoxyethoxyethoxycyclophosphazene] (MEE trimer).

polyphosphazenes are now being investigated as polymer electrolytes for those cells.⁹

To realize efficient DSSCs, the electrolyte must support the transport of both iodide and triiodide ions, which undergo electron transfer reactions at the porous titania anode and transparent conductor cathode, respectively. Generally, liquid electrolytes in DSSCs are composed of an inorganic or organic iodide salt, iodine, and different coadsorbents such as 4-*tert*-butylpyridine, guanidium thiocyanate, and *N*-methylbenzimidazole. It is also generally known that Li⁺ cations can intercalate or adsorb on TiO₂ surfaces and affect the electron transport within the semiconductor film.¹⁰ Thus, the ideal polyphosphazene electrolyte system for DSSCs should promote the dissociation of Li⁺ salts of I⁻ and I₃⁻ and may also incorporate additives that passivate or modulate the energy of trap states at the TiO₂ surface.

In a preliminary study of polyphosphazene-based DSSC electrolytes, we chose methoxyethoxyethoxypolyphosphazene (MEEP, Figure 1a) and hexa(methoxyethoxyethoxy)cyclophosphazene (MEE-trimer, Figure 1b) as model systems.¹¹ MEEP is a thermoplastic polymer. The MEE-trimer is liquid but has negligible vapor pressure at room temperature. Cells

* Corresponding author. E-mail: tem5@psu.edu.

[†] Department of Chemistry.

[‡] Department of Engineering Science and Mechanics.

[§] Department of Electrical Engineering.

were fabricated and tested with LiI/I_2 dissolved in both MEEP and MEE-trimer electrolytes. The performance of these DSSCs was found to depend both on the manner in which the polymer was infiltrated into the porous TiO_2 layer and on the microstructure of the TiO_2 itself. Not surprisingly, liquid MEE-trimer gave higher photocurrents than the solid MEEP electrolyte with LiI/I_2 electrolytes. Interestingly, the conductivity of these electrolytes increased with added I_2 ; the DSSCs nevertheless gave low photocurrents and power conversion efficiencies, consistent with the relatively low ionic conductivity of the polymer/ LiI/I_2 system.

In the present study, we examined MEE-trimer electrolytes containing iodine and different iodide salts (LiI , NaI , NH_4I , and 1-propyl-3-methylimidazolium iodide). We also performed a comparison study on thermoplastic polymer/plasticizer blends of MEEP (Figure 1b)/PC and poly(ethylene oxide) (PEO)/PC. The ion transport properties of these electrolytes are characterized by measuring the total ionic conductivity and the mass-transport-limited anodic and cathodic current for electrolysis of I^- and I_3^- , which provides a measure of the individual ionic conductivities. These measurements also give by difference the cation conductivity in the MEEP/salt and MEE-trimer/salt systems. These measurements are correlated with the current–voltage behavior of DSSCs containing the same electrolyte/salt mixtures. These measurements give some insight into the factors that limit the photocurrent and efficiency in DSSCs that contain phosphazene-based electrolytes and suggest ways in which the composition of the electrolytes might be optimized for improved cell performance.

Experimental Section

Materials. For all phosphazene reactions, hexachlorocyclophosphazene, $(\text{NPCl}_2)_3$ (Fushimi Chemical and Pharmaceutical Co. Ltd., Japan, and Nippon Fine Chemicals), was used as the starting material. The small-molecule cyclic intermediate was purified by recrystallization from heptane and sublimation at 40 °C and 0.05 mmHg vacuum. Celite, sodium metal, and di(ethylene glycol)methyl ether were obtained from Aldrich. Diethyl ether, hexanes, tetrahydrofuran (THF), and methylene chloride (CH_2Cl_2) were purchased from VWR. Di(ethylene glycol) methyl ether was purified by vacuum distillation over calcium hydride. The diethyl ether, hexanes, THF, and CH_2Cl_2 were purified through copper/silica catalytic drying columns. For DSSCs, *cis*-bis(isothiocyanato)bis(2,2'-bipyridyl-4,4'-dicarboxylato)ruthenium(II) bis(tetrabutylammonium) ($\text{RuL}_2(\text{NCS})_2\text{-2TBA}$ also known as Ruthenium535 bis-TBA, or N719) was received from Solaronix and used without purification. Lithium iodide (LiI , Aldrich), sodium iodide (NaI , Aldrich), ammonium iodide (NH_4I , Aldrich), 1-propyl-3-methylimidazolium iodide (PMII, $\text{C}_7\text{H}_{13}\text{IN}_2$, Aldrich), iodine (I_2 , Aldrich), 4-*tert*-butylpyridine ($\text{C}_9\text{H}_{13}\text{N}$, Aldrich), poly(ethylene oxide) ($(\text{CH}_2\text{O})_n$, $M_n = 100\,000$ and $600\,000$, Aldrich), and propylene carbonate (anhydrous, Aldrich) were used as received.

Preparation of Electrodes. The nanocrystalline (nc)- TiO_2 particle slurry was synthesized according to previously published procedures.¹² Electrodes were fluorine-doped tin oxide-coated glass substrates (FTO-glass, TEC8, Hartford Glass Co., Inc., 8 Ω/sq). FTO substrates (1 in. \times 1 in.) were cleaned by sonication for 20 min in isopropanol and for 20 min in ethanol, followed by rinsing with deionized water and drying with air. A few drops of nc- TiO_2 paste were deposited and spread onto the conductive side of the FTO/glass. Cellophane tape spacers with a thickness of 50 μm were applied to opposite edges of the electrode to control the thickness of the doctor-bladed nc- TiO_2 films. The

samples were then calcined at 450 °C for 30 min. The average thickness of TiO_2 film was measured by the profilometer and was between 7 and 8 μm . After the samples had cooled to 150 °C, they were taken out of the furnace and immersed slowly into a 0.3 mM solution of N719 dye in a mixture (50:50) of acetonitrile and *tert*-butanol to prevent cracking of TiO_2 and the substrate. All samples were sensitized for 48 h. After sensitization, the active area of the TiO_2 film was made to be 0.25 cm^2 by scraping away the excess. Stretched parafilm was used as a 20–30 μm spacer between the anode and platinum counter electrode. A drop of the redox electrolyte (see below) was placed on top of the active area, and a platinized FTO-glass counter electrode was placed on it and secured using binder clips. Counter electrodes were made by depositing a few drops of 5 mM hexachloroplatinic acid in anhydrous isopropanol onto 15 Ω FTO-coated glass slides, which were dried and calcined at 385 °C for 15 min. DSSCs samples with electrolytes were assembled in the ambient environment.

Synthesis of MEE-Trimer and MEEP. MEE-trimer and MEEP were synthesized using previously published procedures.^{13–15}

Preparation of Electrolytes. Electrolytes were prepared with different salts at different concentrations, but in all cases the molar ratio of I^- to I_2 was kept at 10:1.

MEE Trimer. The salts and MEE-trimer were mixed and stirred at ambient temperature for 24–48 h. For LiI and NaI at the highest concentrations tested (1 and 1.5 M) the mixtures were heated at ~ 60 °C to more completely dissolve the salt in the MEE-trimer. The solutions were then allowed to cool to room temperature, and iodine was added. Despite the heating procedure, there were still a few crystallites of salts remaining in the MEE-trimer at the highest concentrations. All electrolytes also contained 0.6 M 4-*tert*-butylpyridine.

MEEP/Propylene Carbonate (PC). 1 g of MEEP and 1 g of propylene carbonate (50:50 wt %) were first mixed in a vial. PMII (1 M), I_2 (0.1 M), and 4-*tert*-butylpyridine (0.4 M) were then added and stirred overnight to ensure homogeneity. The MEEP/PC electrolytes were used within 24–48 h of preparation.

PEO100K (or PEO600K)/Propylene Carbonate (PC). 1 g of PEO and 1 g of propylene carbonate (50:50 wt %) were first mixed in a vial. PMII (1 M), I_2 (0.1 M), and 4-*tert*-butylpyridine (0.4 M) were then added, and the mixture was stirred overnight. (Sonication of the PC/PEO mixtures was avoided because it can cause phase separation of the PEO/PC mixture.) These electrolytes were used within 24 h of preparation to avoid phase separation.

Electrochemical Measurements. Photoelectrochemical current–voltage curves of DSSCs were obtained at an irradiation level of 100 mW/cm^2 using AM 1.5 filters. A 150 W Xe Lamp (Oriol, model 77250) was used as the light source and was calibrated with an NREL-certified Si solar cell. Electrical contact was made at the ends of the electrodes using alligator clips, and the cell was connected to a source meter (Keithley, model 2300).

The ionic conductivity of the electrolytes was measured with a HP 4192A impedance analyzer at ambient temperature in a two-point liquid or solid conductivity cell. The apparent diffusion coefficients (D_{app}) of I^- and I_3^- were obtained by measuring steady-state current–voltage curves using a Pt ultramicroelectrode (EE016, Cypress Systems, diameter = 10 μm) as a working electrode and a Pt wire as a counter electrode at a scan rate of 10 mV/s on a CH Instruments potentiostat (model 660). The active radius of the working electrode ($r = 4.67 \mu\text{m}$) was calculated by standardization with 10 mM ferrocene and 0.1 M tetrabutylammonium perchlorate

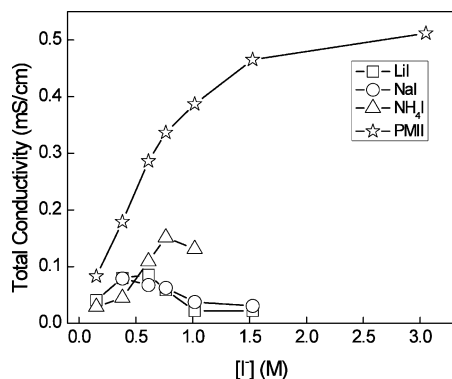


Figure 2. Total conductivity of different iodide/ I_2 salt mixtures (10:1 molar ratio of I^- to I_2) in MEE-trimer electrolytes as a function of salt concentration.

in acetonitrile using a diffusion coefficient of $2.37 \times 10^{-5} \text{ cm}^2/\text{s}$ for ferrocene.¹⁶

Electrochemical impedance spectroscopy (EIS) on DSSCs was performed under 1 Sun irradiation at the open circuit voltage and in the dark at a forward bias (as indicated in Figures 8 and 11) using a Solartron 1260 impedance analyzer in a two-electrode system. The open-circuit voltage was separately measured. The frequency range for the analysis was from 200 K to 0.002 Hz, and the amplitude of the alternating signal was 10 mV. The impedance spectra were fitted with the Zview program from Scribner Associates, Inc.

Results and Discussion

Ionic Conductivity and D_{app} of Different Iodides in MEE-Trimer. The ionic conductivity of different iodide/tri-iodide salt mixtures in MEE-trimer was determined by EIS measurements. The bulk resistance of electrolytes can be obtained from the oblique line at high frequency that intercepts the real axis in the Nyquist plot. The conductivity σ is inversely related to the real part of the bulk impedance (Z) according to eq 1

$$\sigma = \frac{L}{ZA} \quad (1)$$

Figure 2 shows that for all salts, at very low concentration, the conductivity increases with increasing concentration. In the case of the PMII cation, the increase in conductivity is linear up to about 0.7 M as expected for soluble electrolytes. Above 1.0 M concentration the conductivity begins to saturate, consistent with increased ion pairing, and there is only a small increase in conductivity between 1.5 and 3.0 M. In the case of all the other iodide salts, the conductivity quickly saturates and then decreases at salt concentrations above about 0.5 M. This suggests that, for the smaller cations, ion pairing is significant at relatively low concentrations (0.3–0.5 M). The neutral ion pairs and clusters that form at these concentrations do not contribute to conduction.¹⁷ At higher salt concentration, electrostatic cross-linking of the polymer substantially reduces the diffusion coefficients of free M^+ and I^- ions. NH_4I was not soluble in MEE-trimer beyond the concentration of 1 M. For NaI and LiI, the viscosity of the electrolytes increased dramatically above the concentrations of 1 M, consistent with the electrostatic cross-linking mechanism.¹⁸ The striking difference between the behavior of PMII and the alkali iodides suggests that the cations interact differently with the MEE-trimer. The smaller cations are likely to coordinate more strongly to oxygen atoms of the ether side chains of the MEE-trimer than the larger PMII cation.¹⁹

The measured ionic conductivity is determined by both cations and anions in electrolytes, but in the case of the DSSC the transport of the anions (I^- and I_3^-) is the most important factor. The individual conductivities of the electroactive anions can be extracted from the total ion conductivity in order to provide a better understanding of how each ion influences the photovoltaic characteristics of DSSCs.²⁰ The total conductivity can be expressed as the sum of contributions from the individual ions according to eq 2:

$$\sigma(T) = \sum_i \frac{|Z_i|^2 F c_i e D_i}{k_B T} \quad (2)$$

where Z_i , c_i , e , and D_i are the charge, concentration, electronic charge, and diffusion coefficient of the i th ion, T is the absolute temperature, and k_B and F are the Boltzmann and Faraday constants, respectively.²¹ In order to calculate the conductivity of individual ions using this equation, the apparent diffusion coefficients of I^- and I_3^- must be measured.

The apparent diffusion coefficients of electroactive anions can be obtained by measuring electrolysis currents under mass transport-limited conditions. Here, this was done by linear sweep voltammetry using ultramicroelectrodes. Figure 3 shows $I-V$ curves of each electrolyte obtained under quasi-steady-state conditions using 10 μm diameter Pt ultramicroelectrodes. The anodic and cathodic plateau currents were used to calculate the diffusion coefficients (D_{app}) of I^- and I_3^- according to eq 3

$$D_{\text{app}} = \frac{I_{\text{ss}}}{4nCrF} \quad (3)$$

where n is a number of electrons per molecule, C is the bulk concentration, r is the radius of the electrode, and F is the Faraday's constant. While the values of D_{app} obtained by this technique assume that C is equal to the analytical concentration of electrolyte (clearly not valid for the alkali halides, which show strong evidence of ion pairing), the product $D_{\text{app}}C$ ($= D_i c_i$ in eq 2) can be obtained directly from the current and used to calculate the contribution of each ion to the total conductivity.

From Figure 3a, it is evident that the steady state currents for I^- oxidation and I_3^- reduction vary dramatically with different solvents. LiI/ I_2 in acetonitrile exhibits the highest steady-state currents, followed by LiI/ I_2 in propylene carbonate, consistent with the relative viscosities (0.34 and 2.51 cP at 298 K, respectively) of the two solvents. LiI/ I_2 in MEE-trimer shows dramatically lower current for I^- oxidation and I_3^- reduction—about 500 times lower than the current observed in acetonitrile—which is a combined effect of the greater viscosity of the MEE-trimer at high salt concentration and the ion pairing effect noted above. Figure 3b compares on an expanded scale the limiting currents of different iodide salts at same concentrations in MEE-trimer. The currents for both I^- oxidation and I_3^- reduction are highest with the PMII cation, consistent with the total conductivity values shown in Figure 2. Interestingly, higher anodic and cathodic limiting currents are obtained with NaI/ I_2 and NH_4I / I_2 than with LiI/ I_2 , despite the fact that the total conductivities are comparable for the Li and Na salts (Figure 2). This appears to be a consequence of the higher cationic conductivity of Li^+ relative to Na^+ . Again, it is important to note that the performance of the DSSC should depend primarily on the anionic conductivity.

Limiting anodic and cathodic currents were measured at different concentrations in MEE-trimer for each of the iodide

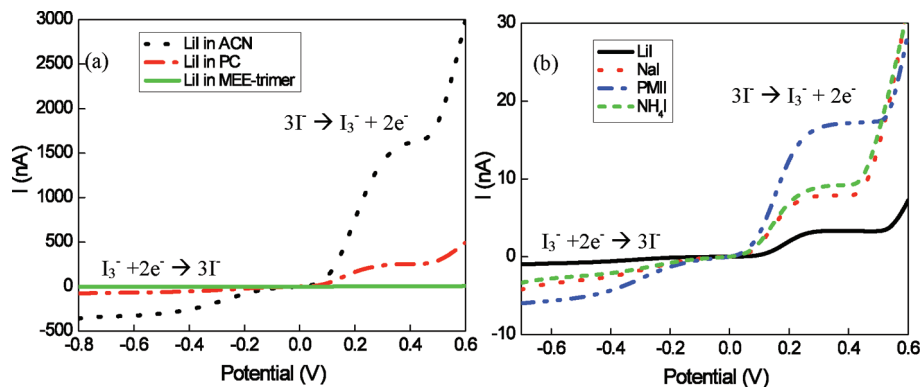


Figure 3. Steady-state voltammograms of the different iodide salts in MEE-trimer. (a) LiI/I₂ in acetonitrile, propylene carbonate, and MEE-trimer. They all contain 1 M LiI, 0.1 M I₂, and 0.6 M 4-*tert* butylpyridine. (b) 1 M LiI, NaI, NH₄I, and PMII, 0.1 M I₂, and 0.6 M 4-*tert*-butylpyridine in MEE-trimer.

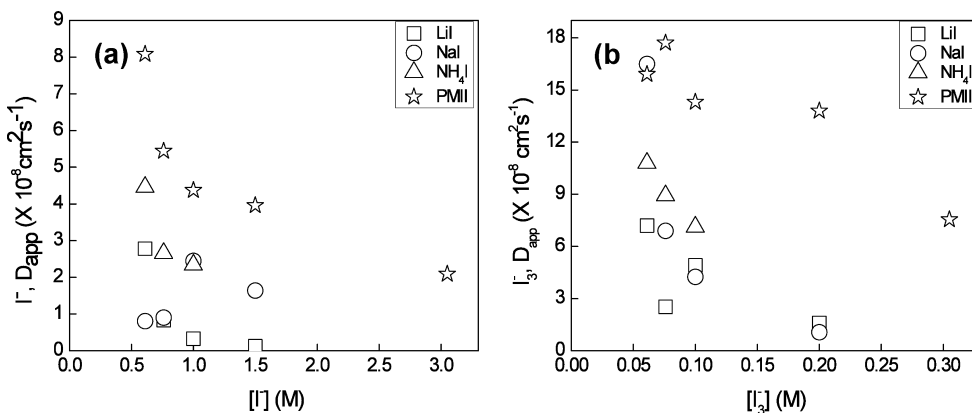


Figure 4. Apparent diffusion coefficients of I⁻ and I₃⁻ from mass transport-limited currents of iodide salts/I₂ in MEE-trimer vs the analytical concentration of I⁻ and I₃⁻. The salt/I₂ mole ratio was 10:1 in all experiments.

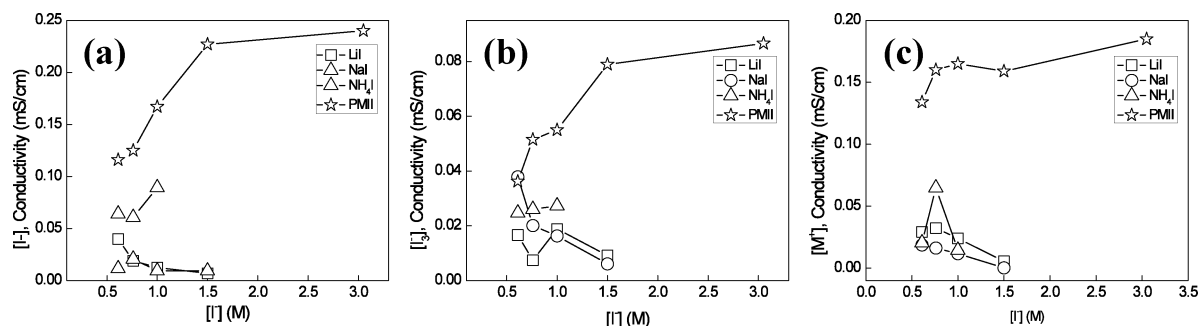


Figure 5. Individual ion conductivities in MEE-trimer electrolytes as a function of salt concentration. The salt/I₂ mole ratio was 10:1 in all cases.

salts. Figure 4 shows the data expressed as the apparent diffusion coefficients (D_{app}) of I⁻ and I₃⁻, with the assumption that I₂ is quantitatively converted to I₃⁻. The general trend is that D_{app} decreases for both I⁻ and I₃⁻ at increasing salt concentration, which is again likely to be a combined effect of increasing ion pairing and viscosity.

From these data and the conductivity data in Figure 2, it is possible to extract the contributions of the anions and cations to the total conductivity. Figure 5 shows that the cations and anions have comparable conductivities, and in all cases (at the 10:1 salt/I₂ molar ratio tested), the transport of I₃⁻ ions is likely to be the limiting factor in MEE-trimer based DSSCs. Interestingly, in this system, LiI is the poorest choice for both I⁻ and I₃⁻ conductivity. NH₄I and NaI give comparable anionic conductivities, which reach optimum values at about 1.0 M salt concentration. The conductivity of all ions is highest in the PMII/I₂ system, where the I₃⁻ conductivity reaches an optimum value at about 1.5 M salt concentration.

Photovoltaic Behavior of DSSCs with Different Iodide Salts in MEE-Trimer Electrolytes. Figure 6a and Table 1 show the photovoltaic behavior of DSSCs containing MEE-trimer electrolytes with different iodide salts at 1.0 M. Electrolytes tested concentrations below 1.0 M showed very poor device efficiency, and the data are not included here. It is evident that the anionic conductivity results are in qualitative agreement with the photovoltaic measurements. The ordering of current densities (PMII > NH₄I > NaI > LiI) matches the ordering of I₃⁻ conductivities at 1.0 M salt concentration. Increasing the PMII concentration while maintaining the 10:1 PMII/I₂ ratio (Figure 6b) also increases the short-circuit current density up to 3.0 M PMII concentration, as anticipated from the trend in anionic conductivity in Figure 5.

In contrast to a distinctive trend observed with the J_{sc} , the V_{oc} did not show a clear pattern among different iodides salts except in the case of LiI. In liquid electrolytes and some polymer electrolytes, different cations have different effects on V_{oc} .²² Li⁺

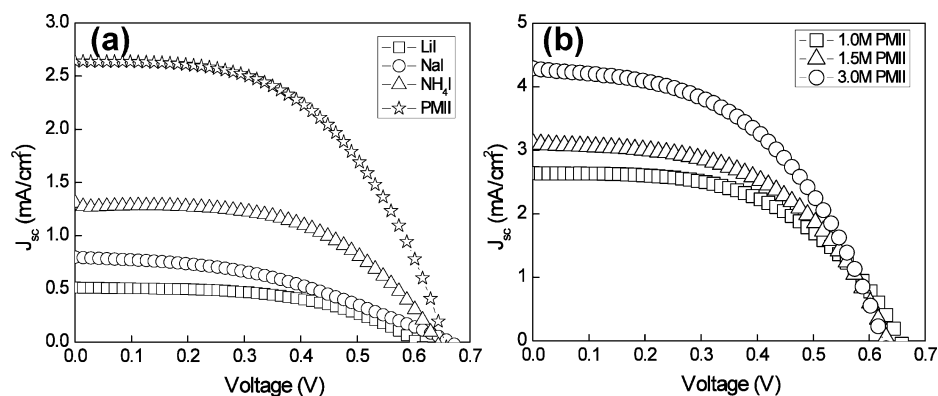


Figure 6. J - V characteristics of DSSCs with different iodide salts in MEE-trimer electrolyte under AM 1.5G illumination. All the electrolytes had a 10:1 salt/ I_2 molar ratio and contained 0.6 M 4-*tert*-butylpyridine.

TABLE 1: Photovoltaic Parameters of DSSCs with Different Iodides in MEE-Trimer under 1 sun (100 mW/cm²)^a

sample	J_{sc} (mA/cm ²)	V_{oc} (V)	ff	P_{max} (mW)	η (%)
LiI	0.51 ± 0.03	0.61 ± 0.01	0.53 ± 0.02	0.041 ± 0.003	0.16 ± 0.01
NaI	0.8 ± 0.1	0.67 ± 0.02	0.41 ± 0.02	0.054 ± 0.008	0.22 ± 0.03
NH ₄ I	1.28 ± 0.03	0.64 ± 0.01	0.55 ± 0.03	0.11 ± 0.01	0.45 ± 0.03
PMII	2.6 ± 0.3	0.655 ± 0.008	0.53 ± 0.02	0.23 ± 0.02	0.92 ± 0.08

^a MEE-trimer = 1.5 g, $[I^-] = 1$ M, $[I_2] = 0.1$ M, and $[TBP] = 0.6$ M. Each entry represents the average of data from five DSSCs.

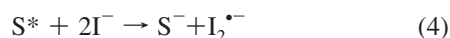
TABLE 2: Photovoltaic Parameters of DSSCs with Different Concentrations of PMII/ I_2 in MEE-Trimer Electrolytes under 1 sun (100 mW/cm²)^a

PMII (M)	J_{sc} (mA/cm ²)	V_{oc} (V)	ff	P_{max} (mW)	η (%)
1.0	2.6 ± 0.3	0.655 ± 0.008	0.53 ± 0.02	0.23 ± 0.02	0.92 ± 0.08
1.5	3.1 ± 0.2	0.633 ± 0.005	0.526 ± 0.008	0.26 ± 0.01	1.03 ± 0.06
3.0	4.3 ± 0.3	0.63 ± 0.01	0.49 ± 0.02	0.33 ± 0.03	1.3 ± 0.01

^a Each entry represents an average of five DSSCs.

can intercalate into the lattice of TiO₂, causing a positive shift of the conduction band edge potential. This increases the driving force for charge injection and typically leads to a higher photocurrent density at the expense of V_{oc} . The effect of Li⁺ on V_{oc} is evident in Figure 6a, but any enhancement in J_{sc} from increased injection efficiency is masked by the lower limiting current of I₃⁻ in the LiI electrolyte.

The photovoltaic properties of DSSCs containing PMII electrolytes at different concentrations are summarized in Table 2. It is clear that J_{sc} increases with increasing concentration of PMII up to 3.0 M, where a power conversion efficiency of 1.3% was observed. V_{oc} starts to drop beyond 1.0 M salt concentration as a result of increased recombination between injected electrons and polyiodide species in the electrolyte. While we did not vary the I₂ concentration in these cells, the conductivity data suggest that adding more iodine may improve the device efficiency slightly; however, strong absorption of I⁻/I₃⁻ in blue region of the spectrum and increasing recombination will limit the device performance. It has been shown by Grätzel and co-workers that in pure PMII electrolytes reductive quenching of the sensitizer (S) by iodide (eq 4) competes with charge injection into TiO₂, resulting in a decrease of photocurrent density by about 20%.²³



Electrochemical Impedance Spectroscopy on MEE-Trimer Electrolytes. To further elucidate the photovoltaic performance of DSSCs containing MEE-trimer electrolytes, the electrochemical impedance spectra were measured in the two-electrode configuration at V_{oc} under 1 sun illumination and under forward

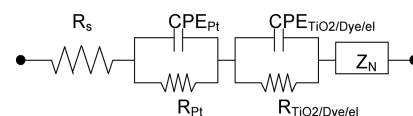


Figure 7. Equivalent circuit of DSSCs with MEE-trimer electrolytes. R_s is total series resistance of the DSSC, which includes the sheet resistance of transparent conductive substrate, electrical contacts, etc. R_{Pt} is the charge transfer resistance at the electrolyte/Pt interface; $R_{TiO_2/Dye/el}$ is the charge transfer resistance at the electrolyte/TiO₂ interface that describes the recombination process; Z_N is the Warburg mass transport impedance of the redox couple in electrolyte. Constant phase elements are used instead of capacitors because of the inhomogeneous current distribution caused by the mesoporosity of the TiO₂ film and the roughness of the Pt counter electrode.

bias in the dark. Figure 7 shows the equivalent circuit that was used to model the impedance of the cell. This simple RC circuit is commonly used to describe the electrochemical process in DSSCs with liquid, polymer, and ionic liquid electrolytes.²⁴ There are typically three arcs in the impedance spectra of DSSCs. The charge transport process at the electrolyte/Pt interface dominates the response at high frequency in the range between 500 000 and 1000 Hz. The arc in the mid-frequency range between 1000 and 1 Hz describes the charge transport process at the TiO₂/dye/electrolyte interface. In the low-frequency region between 1 and 0.002 Hz, the arc represents the mass transport resistance of I₃⁻ in the electrolyte.

Figure 8a shows impedance spectra of different iodide salt/MEE-trimer electrolytes at V_{oc} under 1 sun, and Table 3 lists the fitted values of the resistance associated with each interfacial process in the DSSC. At the V_{oc} under full sun illumination, the device generates no net current since all the injected electrons recombine with I₃⁻, but the oxidized dye is still regenerated by

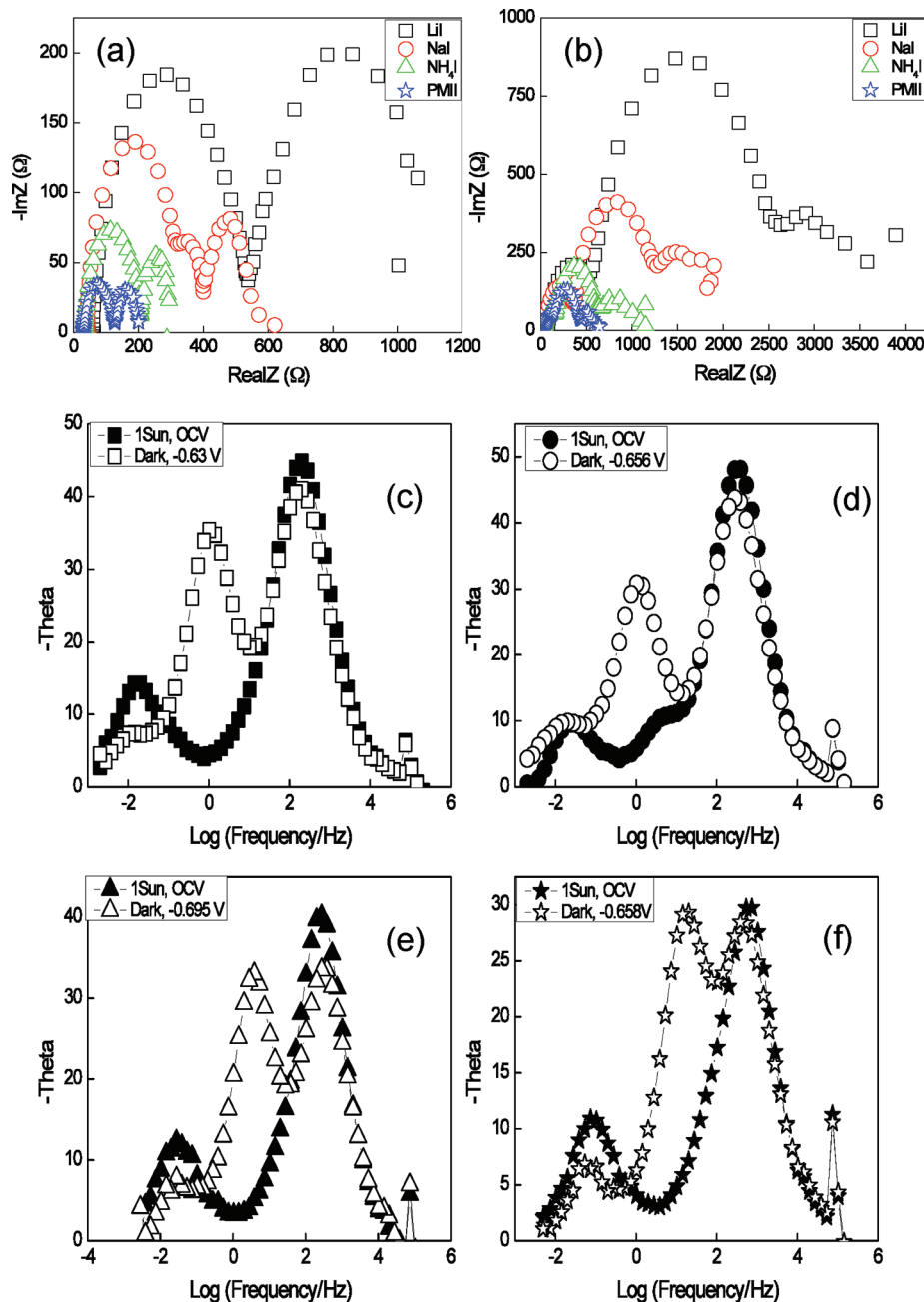


Figure 8. Nyquist plots of DSSCs containing different MEE-trimer electrolytes (a) at V_{oc} under 1 sun and (b) under forward bias in the dark. (c–f) Bode plots of LiI, NaI, NH_4I , and PMII in MEE-trimer electrolytes at V_{oc} under 1 sun and under forward bias in the dark, respectively. All electrolytes contained 1.0 M salt, 0.1 M I_2 , and 0.6 M TBP.

TABLE 3: Internal Impedance Components of DSSCs with MEE-Trimer Based Electrolytes at V_{oc} under 1 sun, Obtained by Fitting the Impedance Spectra

$[\Gamma^-]$	R_{Pt} (Ω)	$R_{\text{TiO}_2/\text{Dye/el}}$ (Ω)	Z_N (Ω)
LiI	452.4		532.5
NaI	278.1	63.64	177.6
NH_4I	116.2	37.43	121.6
PMII	91.68		78.95

Γ^- .^{24a} As shown in Figure 8a, the charge transfer resistance at the Pt/electrolyte interface, which is the diameter of the first arc, increases in the order $\text{PMII}^+ < \text{NH}_4^+ < \text{Na}^+ < \text{Li}^+$. The high charge transfer resistance at the Pt electrode indicates the slow regeneration of Γ^- from I_3^- , which will then result in low J_{sc} . In order to verify that the first arc is indeed caused by charge transfer resistance at the Pt/electrolyte interface, MEE-trimer

electrolytes were placed between the two Pt electrodes and EIS spectra were obtained at 0 V in the same frequency range used for DSSCs (Figure 9). Indeed, the arcs in these spectra match quite well with those obtained in the high- and low-frequency regimes of the spectra measured with DSSCs.

Interestingly, the mid-frequency arcs of MEE-trimer electrolytes were hard to distinguish in the spectra. It appears that the charge transfer resistance at the Pt/electrolyte interface overwhelms the charge transfer resistance at the $\text{TiO}_2/\text{dye}/\text{electrolyte}$ interface. For DSSCs with high efficiencies, the electron transport resistance within the TiO_2 film is much smaller, compared to the recombination resistance at the $\text{TiO}_2/\text{dye}/\text{electrolyte}$ interface. It is generally assumed that the mid-frequency arc mainly describes the recombination process between electrons in TiO_2 and the electrolyte, and an enlarged mid-frequency arc represents a reduced recombination process.

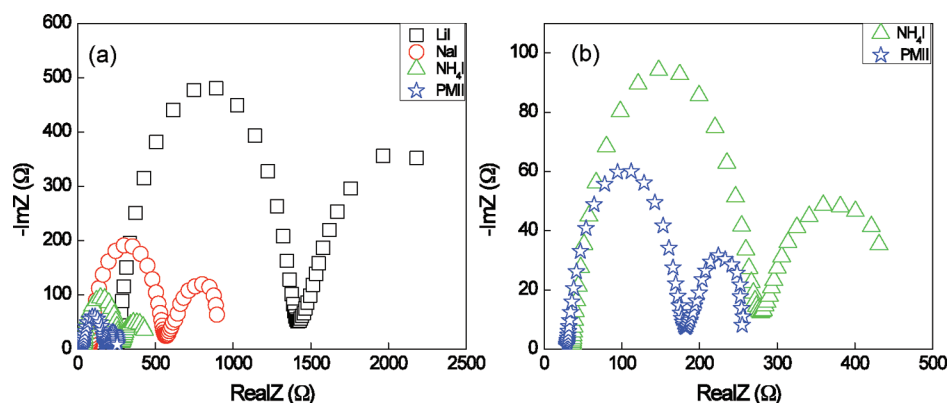


Figure 9. (a) Nyquist plots of MEE-trimer electrolytes between two Pt electrodes at 0 V dc bias with 10 mV ac voltage. (b) Enlarged Nyquist plot of NH₄I and PMII in MEE-trimer. The same concentrations of redox couples were used as in Figure 8.

TABLE 4: Internal Impedance Components of DSSCs with MEE-Trimer Based under Forward Bias in the Dark, Obtained by Fitting the Impedance Spectra

[I ⁻]	R_{Pt} (Ω)	$R_{TiO_2/Dye/el}$ (Ω)	Z_N (Ω)
LiI	440	1635	1333
NaI	298	731	842
NH ₄ I	148	495	356
PMII	101	270	206

In MEE-trimer electrolytes, because of slow transport of I⁻/I₃⁻, recombination between the oxidized dye molecules and electrons in TiO₂ may also play a role, resulting in a lower photocurrent yield and J_{sc} . In conventional liquid electrolytes, the major recombination pathway is at the TiO₂/electrolyte interface since the dye regeneration process is very effective. Hence, in MEE-trimer electrolytes, there may be more than one major recombination pathway that affects the device performance.

The arc observed at a low-frequency region corresponds to the mass transport resistance of I₃⁻ in the electrolyte. In low-viscosity liquid electrolyte systems, because of the high ionic conductivity and mobility of both I⁻ and I₃⁻ ions, Z_N is small compared to the other internal resistances of the DSSCs and is hard to observe it in the Nyquist plot.²⁵ However, in viscous electrolytes such as MEE-trimer, it is easy to determine Z_N . The arcs of MEE-trimer electrolytes expand in the same order as the charge transfer resistance at the Pt/electrolyte interface. These measurements are consistent with the measurements of individual ion conductivities by linear sweep voltammetry.

Figure 8b and Table 4 show the results of impedance measurements and fitted impedance values for DSSCs that were measured in the dark with a forward bias. In the dark, when a forward bias is applied to the DSSC, electrons transport through the TiO₂ and react primarily with I₃⁻ as I⁻ is oxidized to I₃⁻ at the counter electrode.^{24a} In the dark, all three arcs of DSSCs are evident in the Nyquist plots of MEE-trimer cells, in contrast to the data obtained at V_{oc} under full illumination. Figure 8c–e shows Bode plots of these electrolytes under 1 sun and in the dark, and the difference can be very clearly seen. This difference can be explained by comparing the local concentration of I₃⁻ on TiO₂ films at open circuit and under forward bias. Under illumination at open circuit, I₃⁻ is formed by dye regeneration in close proximity to the TiO₂/electrolyte interface, whereas in the dark, I₃⁻ is generated at counter electrode and diffuses through the electrolyte to the TiO₂ film.^{24a} This provides an explanation of a clear distinction of the mid-frequency arc from the first arc at the high-frequency region. At open circuit under illumination, both I⁻ and I₃⁻ are present at their bulk concentrations at the TiO₂/dye/electrolyte interface. The mid-frequency

TABLE 5: Total Ionic Conductivity of MEEP/PC, PEO (Average $M_v = 100K$)/PC, and PEO (Average $M_v = 600K$)/PC

sample	ionic conductivity (mS/cm)
MEEP/PC	2.7
PEO100K/PC	1.7
PEO600K/PC	0.71

arc is not distinguishable and sometimes missing from the spectra, indicating a small charge transfer resistance at the TiO₂/dye/electrolyte interface relative to other impedance components of the cell. Under forward bias in dark, however, the mid-frequency arc expands as the concentration of I₃⁻ is depleted at the interface.

The photovoltaic measurements together with the impedance spectra demonstrate that the ionic conductivity is not the only factor that determines the performance of DSSCs with the MEE-trimer electrolytes. The impedance spectra suggest that minimizing the recombination process is also an important problem with viscous electrolytes such as the MEE-trimer. To reduce the rate of recombination at the TiO₂/dye/electrolyte interface, coating the TiO₂ particles with a thin layer of oxides that have a more negative conduction band edge potential than TiO₂ can create an energy barrier, which in this case may minimize these recombination reactions and increase the device efficiency.²⁶

Polyphosphazene/Propylene Carbonate vs Poly(ethylene oxide)/Propylene Carbonate. Having identified PMII as the best iodide salt for MEE-trimer based electrolytes, a high polymeric polyphosphazene thermoplastic thermoplastic gum (MEEP) with a small molecule plasticizer (propylene carbonate, PC) was examined as an alternative electrolyte. It was evaluated against poly(ethylene oxide)/PC with a molecular weight close to the MEEP used in the study. PC was chosen as the plasticizer because of its low volatility relative to acetonitrile. We have found that using acetonitrile to dissolve the electrolyte and polymer, followed by vacuum drying to remove the solvent, gives inconsistent DSSC performance results. This is because of variable loss of the volatile solvent and iodine during the heating/vacuum-drying process. Because the boiling point of propylene carbonate (240 °C) is much higher than that of acetonitrile, it can be used as a plasticizer without complications arising from volatility.

Table 5 summarizes the ionic conductivity of MEEP/PC (50:50 wt %) and PEO/PC (50:50 wt %) blends. MEEP/PC shows higher ionic conductivity than PEO/PC blends. MEEP/PC forms a homogeneous mixture which is stable for at least 1 month, whereas PEO/PC did not appear to be a homogeneous mixture within a few days after its preparation. The poor phase stability

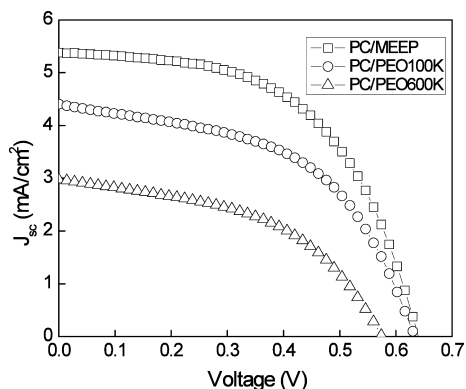


Figure 10. J - V characteristics of DSSCs with MEEP/PC and PEO100K (and PEO600K)/PC blends under the AM 1.5G illumination. All electrolytes contain 1.0 M PMII, 0.1 M I_2 , and 0.4 M 4-*tert*-butylpyridine.

of PEO/PMII/PC relative to the analogous MEEP mixtures may be a result of the tendency of PEO to crystallize.²⁷

Photovoltaic measurements were carried out on these electrolytes (Figure 10), and their photovoltaic parameters are listed in Table 6. The MEEP/PC electrolyte shows better photovoltaic performance than the PEOs/PC mixtures. The ordering of J_{sc} values with these electrolytes is in accord with the ionic conductivity measurements. MEEP/PC also gave a higher fill factor than the PEO/PC electrolytes. Electrochemical impedance spectra (Figure 11) reveal that the PEO/PC mixtures have much higher internal resistance compared to the MEEP/PC electrolytes, resulting in a lower fill factor. The Warburg mass transport resistance of the PEO/PC electrolyte in the low-frequency region is significantly higher than that of MEEP/PC. This suggests that the transport of I_3^- in PEO/PC is slower, possibly due to phase separation in the electrolyte. The slow ion transport also affects the dye regeneration, which can lower the J_{sc} and can create a concentration polarization loss in the cell.²⁸ It may be possible to improve the characteristics of the MEEP/PC system by varying amount of I_2 and adding inorganic nanofillers such as TiO_2 and SiO_2 particles to enhance the mechanical stability and

the conductivity of the electrolyte.²⁹ Experiments along these lines are currently in progress.

Conclusions

A series of phosphazene-based nonvolatile electrolytes with different iodide salts were examined by linear sweep voltammetry and electrochemical impedance spectroscopy. The results illustrate that the conductivity of individual anions (I^- and I_3^-) in MEE-trimer based electrolytes is strongly cation-dependent. A high concentration of iodide salt and I_2 is needed to lower the electrolyte impedance and also to efficiently regenerate the oxidized sensitizer, but it also increases the recombination rate. We find that PMII is a better iodide source for MEE-trimer electrolytes than LiI, NaI, or NH_4I . Interestingly, this is the opposite of the trend observed with the more widely studied PEO polymer electrolytes for DSSCs. MEEP polymer/PC-based DSSCs containing the PMII electrolyte have transport behavior that closely resembles that of the MEE-trimer/PMII DSSCs. Although the power conversion efficiency is currently low, the amorphous nature of the MEEP polymer and the improved photovoltaic performance relative to PEO are encouraging. Because it is easy to vary the side groups of polyphosphazenes, these polymers can be easily redesigned for DSSCs applications. Understanding the loss mechanisms in polyphosphazene-based DSSCs should inform future studies in which oligomeric or monomeric phosphazenes are used as nonvolatile liquid electrolytes. We are currently investigating the possibility of making room temperature ionic liquids based on phosphazenes that could serve as both the solvent and the iodide salt in DSSCs.

Acknowledgment. This work was supported by the U.S. Department of Energy under contract DE-PS36-07GO97025. We thank Prof. Mary Beth Williams and Carl P. Myers for providing access to equipment in their laboratory.

References and Notes

- (1) Chen, C.-Y.; Wang, M.; Li, J.-Y.; Pootrakulchote, N.; Alibabaei, L.; Ngoc-le, C.; Decoppet, J.-D.; Tsai, J.-H.; Grätzel, C.; Wu, C.-G.; Zakeeruddin, S. M.; Grätzel, M. *ACS Nano* **2009**, *3*, 3103.

TABLE 6: Photovoltaic Parameters of DSSCs with MEEP/PC vs PEO/PC under 1 sun (100 mW/cm^2)^a

sample	J_{sc} (mA/cm ²)	V_{oc} (V)	ff	P_{max} (mW)	η (%)
MEEP/PC	5.4 ± 0.2	0.640 ± 0.004	0.55 ± 0.02	0.471 ± 0.007	1.88 ± 0.03
PEO100K/PC	4.4 ± 0.1	0.63 ± 0.01	0.52 ± 0.02	0.36 ± 0.01	1.44 ± 0.06
PEO600K/PC	3.0 ± 0.2	0.58 ± 0.01	0.47 ± 0.05	0.21 ± 0.04	0.8 ± 0.2

^a All entries are average values of multiple samples: MEEP/PC (four samples), PEO600K/PC (four samples), PEO100K/PC (three samples).

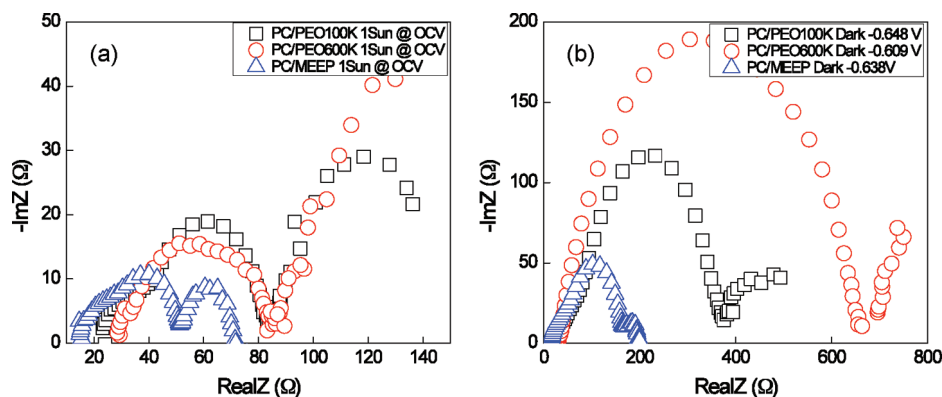


Figure 11. Impedance spectra of DSSCs containing MEEP/PC and PEO100K (and 600K)/PC blends (a) at V_{oc} under 1 sun and (b) under forward bias in the dark.

- (2) Yu, B.; Cao, Y.; Zhang, J.; Wang, M.; Li, R.; Wang, P.; Zakeeruddin, S. M.; Grätzel, M. *Nature Mater.* **2008**, *7*, 626.
- (3) (a) Snaith, H. J.; Zakeeruddin, S. M.; Wang, Q.; Péchy, P.; Grätzel, M. *Nano Lett.* **2006**, *6*, 2000–2003. (b) Snaith, H. J.; Moule, A. J.; Klein, C.; Meerholz, K.; Friend, R. H.; Grätzel, M. *Nano Lett.* **2007**, *7*, 3372.
- (4) O'Regan, B.; Lenzmann, F.; Muis, R.; Wienke, J. *Chem. Mater.* **2002**, *14*, 5023.
- (5) (a) Han, H. W.; Liu, W.; Zhang, J.; Zhao, X.-Z. *Adv. Funct. Mater.* **2005**, *15*, 1940. (b) Stergiopoulos, T.; Arabatzis, I. M.; Katsaros, G.; Falaras, P. **2002**, *2*, 1259. (c) Kim, Y. J.; Kim, J. H.; Kang, M. S.; Lee, M. J.; Won, J.; Lee, J. C.; Kang, Y. S. *Adv. Funct. Mater.* **2004**, *16*, 1753. (d) Kato, T.; Okazaki, A.; Hayase, S. *Chem. Commun.* **2005**, 363. (e) Murai, S.; Mikoshiba, S.; Sumino, H.; Kato, T.; Hayase, S. *Chem. Commun.* **2003**, 1534.
- (6) Gleria, M. *Chem. Ind.* **1988**, *70*, 15.
- (7) Allcock, H. R. *Polym. Prepr.* **2000**, *41*, 553.
- (8) Gleria, M.; De Jaeger, R. *Top. Curr. Chem.* **2005**, *250*, 165.
- (9) Xiang, W.; Zhou, Y.; Yin, X.; Zhou, X.; Fang, S.; Li, Y. *Electrochim. Acta* **2009**, *54*, 4186.
- (10) Wang, H.; Bell, J.; Desilvestro, J.; Bertoz, M.; Evans, G. *J. Phys. Chem. C* **2007**, *111*, 15125.
- (11) Feh, S.-T.; Lee, S.-H. A.; Pursel, S.; Basham, J.; Grimes, C. A.; Horn, M. W.; Mallouk, T. E.; Allcock, H. A., submitted for publication.
- (12) Lee, S.-H. A.; Abrams, N. M.; Hoertz, P. G.; Barber, G. D.; Halaoui, L. I.; Mallouk, T. E. *J. Phys. Chem. C* **2008**, *112*, 14415.
- (13) Lyon, R. E.; Speitel, L.; Walters, R. N.; Crowley, S. *Fire Mater.* **2003**, *27*, 195.
- (14) Nazri, G.; McArthur, D. M.; Ogara, J. F. *Chem. Mater.* **1989**, *1*, 370.
- (15) Xu, K.; Ding, M. S.; Zhang, S.; Allen, J. L.; Jow, T. R. *J. Electrochem. Soc.* **2002**, *149*, A622.
- (16) Clegg, A. D.; Rees, N. V.; Klymwnko, V.; Coles, B. A.; Compton, R. G. *J. Electroanal. Chem.* **2005**, *580*, 78.
- (17) Obeidi, S.; Stolwijk, N. A.; Pas, S. J. *Macromolecules* **2005**, *38*, 10750.
- (18) MacCallum, J. R.; Vincent, C. A. *Polymer Electrolyte Reviews*; Elsevier Applied Science: London, 1987; p 78.
- (19) Park, J. H.; Yum, J.-H.; Kim, S.-Y.; Kang, M.-S.; Lee, Y.-G.; Lee, S.-S.; Kang, Y.-S. *J. Photochem. Photobiol., A* **2008**, *194*, 148.
- (20) Kang, M.-S.; Ahn, K.-S.; Lee, J.-W.; Kang, Y. S. *J. Photochem. Photobiol., A* **2008**, *195*, 198.
- (21) Wang, P.; Zakeeruddin, S. M.; Moser, J. E.; Nazeeruddin, M. K.; Sekiguchi, T.; Grätzel, M. *Nature Mater.* **2003**, *2*, 402.
- (22) (a) Zaban, A.; Ferrere, S.; Gregg, B. A. *J. Phys. Chem. B* **1998**, *102*, 452. (b) Wang, H.; Bell, J.; Desilvestro, J.; Bertoz, M.; Evans, G. *J. Phys. Chem. C* **2007**, *111*, 15125. (c) Liu, Y.; Hagfeldt, A.; Xiao, X. R.; Lindquist, S. E. *Sol. Energy Mater. Sol. Cells* **1998**, *55*, 267. (d) Bhattacharya, B.; Lee, J. E.; Gen, J.; Jung, H.-T.; Park, J.-K. *Langmuir* **2009**, *25*, 3276. (e) Shen, X.; Xu, W.; Xu, J.; Liang, G.; Yang, H.; Yao, M. *Solid State Ionics* **2008**, *179*, 2027. (f) Chatzivasiloglou, E.; Stergiopoulos, T.; Kontos, A. G.; Alexis, N.; Prodromidis, M.; Falaras, P. *J. Photochem. Photobiol., A* **2007**, *192*, 49.
- (23) Wang, P.; Wenger, B.; Humphry-Baker, R.; Moser, J.-E.; Teuscher, J.; Kántlehner, W.; Mezger, M.; Stoyanov, S. V.; Zakeeruddin, S. M.; Grätzel, M. *J. Am. Chem. Soc.* **2005**, *127*, 6850.
- (24) (a) Wang, Q.; Moser, J.-E.; Grätzel, M. *J. Phys. Chem. B* **2005**, *109*, 14945. (b) Adachi, M.; Sakamoto, M.; Jiu, J.; Ogata, Y.; Isoda, S. *J. Phys. Chem. B* **2006**, *110*, 13872. (c) Fabregata-Santiago, F.; Bisquert, J.; Garcia-Belmonte, G.; Boschloo, G.; Hagfeldt, A. *Sol. Energy Mater. Sol. Cells* **2005**, *87*, 117. (d) Longo, C.; Nogueira, A. F.; De Paoli, M.; Cachet, H. *J. Phys. Chem. B* **2002**, *106*, 5925. (e) Fabregat-Santiago, F.; Bisquert, J.; Palomares, E.; Otero, L.; Kuang, D.; Zakeeruddin, S. M.; Grätzel, M. *J. Phys. Chem. C* **2007**, *111*, 6550. (f) Zakeeruddin, S. M.; Grätzel, M. *Adv. Funct. Mater.* **2009**, *19*, 2187.
- (25) Wei, T. W.; Wan, C. C.; Wang, Y. Y. *Sol. Energy Mater. Sol. Cells* **2007**, *91*, 1892.
- (26) (a) Diamant, Y.; Chappel, S.; Chen, S. G.; Melamed, O.; Zaban, A. *Coord. Chem. Rev.* **2004**, *248*, 1271. (b) Dimant, Y.; Chen, S. G.; Melamed, O.; Zaban, A. *J. Phys. Chem. B* **2003**, *107*, 1977. (c) Palomares, E.; Clifford, J.; Haque, S. A.; Lutz, T.; Durrant, J. R. *J. Am. Chem. Soc.* **2003**, *125*, 475.
- (27) (a) Wang, Y. *Sol. Energy Mater. Sol. Cells* **2009**, *93*, 1167. (b) Lan, Z.; Wu, J.; Lin, J.; Huang, M.; Lin, P.; Huang, Y. *Sol. Energy* **2006**, *80*, 1483.
- (28) Lee, C.-P.; Chen, P.-Y.; Vittal, R.; Ho, K.-C. *J. Mater. Chem.* **2010**, *20*, 2356.
- (29) Nei de Freitas, J.; Nogueira, A. F.; De Paoli, M.-A. *J. Mater. Chem.* **2009**, *19*, 5279.